




Characterisation of Gamma-Ray Point-Sources Concealed in Shipping Containers using Image Reconstruction

Euan L. Connolly 
Interface Analysis Centre
University of Bristol
Bristol, UK
e.connolly@bristol.ac.uk

Dean T. Connor 
National Nuclear Laboratory
Chadwick House, Warrington, UK

Peter G. Martin 
Interface Analysis Centre
University of Bristol
Bristol, UK

ABSTRACT

Radiation portal monitors positioned at seaports form a crucial part of national security infrastructure by providing a means to deter and detect the illicit transportation of nuclear and radioactive materials. With around 90% of global goods transported by sea, it is essential that international freight can be rapidly and non-invasively screened for materials that have potential use in radiological dispersal devices or improvised nuclear explosive devices. To maximise detection efficiency, conventional radiation portal monitors use low-cost, large-area scintillator detectors, usually polyvinyl toluene plastic, that maximises the collection of gamma radiation as any concealed sources pass through the portal monitor. While advantageous in many regards, a drawback of using large area scintillators in radiation portal monitors is that they are non-directional; it is impossible to determine the direction from which the measured radiation originates. In this work, an algebraic method called maximum likelihood expectation maximisation (MLEM) reconstruction is applied to simulated data from the non-directional detectors found in conventional radiation portal monitors. The MLEM method is well studied in the field of medical imaging where high resolution, small, and directional detectors are used and has more recently been applied to radiation mapping problems with non-directional detectors. To use the MLEM reconstruction method in shipping container screening the response function of each detector in the radiation portal monitor to a radioactive point-source is first characterised on a regular grid of points in the centre of the portal monitor. Through making assumptions about the cargo, such as homogeneity throughout the shipping container and prior knowledge of the material composition, an attempt is made to include the attenuating effect of the cargo in the detector response function. With the detector response function defined for a given cargo type, three variants of the MLEM method are used to characterise concealed point-sources in the cargo for reference cargo types, including a container filled with scrap metal. Preliminary results show the algorithm is capable of localising the source to within a few voxels in the discretised space in the container and estimating the activity to the correct order of magnitude.

I. INTRODUCTION

Ocean shipping is the dominant transport mode for global trade, with around 90% of traded goods being shipped across the seas [1]. As a result, seaports are critical nodes for international trade and commerce. The large volume of freight passing through seaports every day means they can be targeted by terrorists or criminal organisations seeking to smuggle contraband or dangerous materials into or out of countries. The unauthorised distribution of radioactive or nuclear materials by such means poses threats to national and global security as they could be fabricated into radiological dispersal devices (RDDs) or improvised nuclear explosive devices (INEDs). The detonation of RDDs or INEDs has the potential to cause loss of human life, as well as significant economical and societal damage. Already in 2023 there have been widely reported cases of lost radioactive materials, including a capsule containing ^{137}Cs in Western Australia and tonnes of Uranium in Libya [2][3]. While the materials in questions were recovered, both cases demonstrate how material suitable for use in RDDs or INEDs can be misplaced with the potential to end up in the hands of malicious actors and highlights the need for a robust and sensitive screening procedures to prevent trafficking of such materials through seaports.

Existing infrastructure in place at seaports to screen imports for radioactive materials consists of radiation portal monitors (RPMs) utilising plastic-based scintillators for γ detection and separate neutron detectors, usually ^3He -based [4]. The affordability and large available sizes of plastic scintillators, such as polyvinyl toluene (PVT), make them suitable for detecting γ emitters without disrupting the flow of cargo through the seaport as the large-area detectors can be placed in RPMs straddling multiple traffic lanes. Unfortunately, the energy resolution of PVT scintillators is poor, meaning any detection events that cannot be ruled out as threats using processing techniques such as spectral windowing or template matching [4], must be investigated in a secondary screening phase to identify the isotope(s), activity, and location of the source(s) causing the alarm. Plastic-based RPMs are, therefore, susceptible to false-positive alarms from naturally occurring radioactive material (NORM) and medical sources. As all alarms require costly and time-intensive secondary investigation, there exists a trade-off between maximising detection efficiency and minimising false alarms, which require considerable operational resources.

Proposed methods for screening shipping containers for radioactive materials in the future vary from drone-based screening with modular-spectroscopic radiation detectors, to cosmic muon tomography for special nuclear material detection [5][6]. However, the ability of RPM-based systems to maintain a high throughput of containers with minimal impact on port operation makes it highly likely that screening systems will rely on RPMs in the future. This work considers the data from a PVT-based RPM in combination with an advanced data processing algorithm to demonstrate how the activity and location of a radioactive point-source concealed in a shipping container, as well as the background count-rate, can be accurately characterised. Doing so will contribute to existing algorithms for processing PVT-based RPM data, ultimately helping to minimise false-positive alarms [7].

Specifically, an image reconstruction technique called maximum likelihood expectation maximisation (MLEM), commonly used in reconstruction of PET or SPECT data in medical imaging, is utilised to determine the radioactive source distribution within a shipping container using RPM measurements. The MLEM method is demonstrated for single or multiple radioactive point-source localisation in [8] using a non-directional detector. More recent work using a directional detector has accounted for attenuation in surrounding materials [9]. However, in the case of shipping container screening the detectors are non-directional and the distribution of attenuating cargo within the container is unknown. The non-directionality implies that the range of possible paths and materials

traversed by γ radiation incident onto the detector is not well defined, therefore making it difficult to account for the attenuation in the cargo, container and surrounding materials. One method to address this relies on x-ray radiographic images of the container to estimate the density, and hence the shielding profile of the cargo [10]. However, the use of such active screening techniques may not be feasible in all scenarios. To solve this problem, this work adopts the simplest possible model of cargo in a shipping container and using the variants of the MLEM algorithm described in [8] demonstrates how a point-source concealed in a shipping container can be accurately characterised, accounting for attenuation when the cargo material is known.

II. THEORY

To use image reconstruction methods to determine the distribution of a radioactive source, radiation measurements are expressed in vector notation as;

$$\mathbf{Y} = \mathbf{A} \cdot \mathbf{x} + b\mathbf{t}, \quad (1)$$

where \mathbf{Y} are the mean counts expected in each of the I measurements, \mathbf{x} is the activity distribution of the radioactive source discretised into J voxels within a shipping container, \mathbf{A} is the $I \times J$ projection matrix or detector response function (DRF) that maps the source distribution space onto the measurement space, b is the mean background count-rate for a specified detector, and \mathbf{t} is the vector of measurement times [8]. The goal of a reconstruction algorithm is then to find the solution to the optimisation problem;

$$\hat{\mathbf{x}}, \hat{b} = \underset{\mathbf{x}, b}{\operatorname{argmin}} \ell(\mathbf{x}, b|\mathbf{y}) + \beta R(\mathbf{x}), \quad (2)$$

where $\hat{\cdot}$ represents the optimum values, and ℓ is the negative log-likelihood of the radioactive source distribution given the measurements, \mathbf{y} . The second term in (2) is comprised of a weight factor, β , and a penalty function, $R(\mathbf{x})$, which is used to incorporate *a priori* knowledge of the source distribution into the solution. For the detection of point-like radiation sources, a sparse solution is desirable. A penalty function found to produce sparser solutions than the unpenalised algorithm when reconstructing a source distribution from measurements obtained with a Compton-imaging detector is proposed in [11], and has the form;

$$R(\mathbf{x}) = \sum_j \log\left(\frac{x_j}{\delta} + 1\right), \quad (3)$$

where δ is a scale factor.

The counts in each measurement, y_i , are the sum of independent Poisson random variables, $N_{ij} \sim \text{Poisson}(a_{ij}x_j)$ and $B_i \sim \text{Poisson}(bt_i)$. As a result, the negative log-likelihood can be expressed as;

$$\ell(\mathbf{x}, b; \mathbf{y}) = -\log(P(\mathbf{y}; \mathbf{x}, b)) = \sum_i \sum_j a_{ij}x_j - N_{ij} \log(a_{ij}x_j) + \sum_i bt_i - B_i \log(bt_i), \quad (4)$$

where the factorial terms in the respective summations have been ignored as they are independent of \mathbf{x} and b . To extend the method to account for attenuation in a given medium N_{ij} is updated to $N_{ij} \sim \text{Poisson}(a_{ij}e^{-\mu_g \rho r_{ij}} x_j)$ where ρ is the medium density, μ_g is the mass attenuation coefficient of the medium, and r_{ij} is an average distance through the medium from the j 'th voxel to the detector in the i 'th measurement [9][12].

Incorporating the attenuation factor into the DRF, the iterative update equations can be derived from (4) and for the unregularised MLEM method are given by;

$$\hat{\mathbf{x}}^{k+1} = \frac{\hat{\mathbf{x}}^k}{\mathbf{A}^T \cdot \mathbf{1}} \otimes \left[\mathbf{A}^T \cdot \frac{\mathbf{y}}{\mathbf{A} \cdot \hat{\mathbf{x}}^k + \hat{b}^k \mathbf{t}} \right], \quad (5)$$

and

$$\hat{b}^{k+1} = \frac{\hat{b}^k}{\mathbf{t}^T \cdot \mathbf{1}} \left[\mathbf{t}^T \cdot \frac{\mathbf{y}}{\mathbf{A} \cdot \hat{\mathbf{x}}^k + \hat{b}^k \mathbf{t}} \right], \quad (6)$$

where k is the iteration number. In addition to unregularised MLEM, regularised MLEM with the penalty function (3) and a point-source MLEM (MLEM PS) variant are compared. The iterative update equations for the regularised MLEM algorithm are derived in [11]. The point-source variant, proposed in [8], solves (2) with no regularisation for a single voxel, zeroing the activities in every other voxel and returning the optimum point-source solution.

III. DATA SIMULATION AND ALGORITHM IMPLEMENTATION

A. Simulated RPM Data

Figure 1 depicts the model of the RPM and the transiting shipping container used in this work. The PVT-based RPM is modelled as four $60 \times 3.8 \times 203$ cm (L \times W \times H) PVT panels, with 5 m between the faces of the two panels on either side of the RPM.

A standard 20 ft shipping container is modelled as a cuboid shell with external dimensions $606 \times 243 \times 259$ cm and 5 mm wall thickness. Within the container, cargo is modelled as a homogeneous cuboid with dimensions equal to the maximum internal dimensions of a standard container, $587 \times 233 \times 235$ cm [13]. Three cargo compositions are considered: no cargo; iron cargo at 0.2 gcm^{-3} , approximately the average loaded container density; and iron cargo at 0.6 gcm^{-3} , close to the density limit for a loaded container [14]. With 28% of containerised commodities imported into the US in 2006 being metal based, iron represents a likely cargo and the homogeneously distributed cargo could represent scrap metal, machine parts, or transportation equipment [14].

To represent the characteristic emission from ^{137}Cs , which finds widespread use in industry and medical applications in TBq quantities, a 662 keV γ source is modelled as a 2.5 cm sphere [15]. The source is positioned within the cargo at the center, mid, and corner positions indicated in the technical drawings in Figure 1.

The GEANT4 simulation toolkit is used to determine the number of counts measured by the PVT detectors as the shipping container passes through the RPM [16]. The model of the RPM, container, cargo, and source are defined in GEANT4 as described in the above paragraphs, and the container position within the RPM is varied. Measurements are simulated in the region where the source position lies within 2.5 m of the RPM center; at a transit speed of 1.2 ms^{-1} (4.3 kmhr^{-1}) this corresponds to 41 measurements, each separated by 0.1 s (12 cm). At each measurement position 10^7 (no cargo) or 10^8 (0.2 and 0.6 gcm^{-3} cargo) initial 662 keV γ s are generated in GEANT4 and tracked through the geometry.

B. RPM Detector Response Function

For every measurement, the j 'th element of the DRF describes the fraction of radiation emitted from the j 'th voxel that registers as a count in the detector. This is approximated by;

$$A_j = \epsilon_j^G \epsilon_j^I \exp(-\bar{l}_j^{\text{wall}} \rho^{\text{iron}} \mu_g^{\text{iron}}) \exp(-\bar{l}_j^{\text{cargo}} \rho^{\text{cargo}} \mu_g^{\text{cargo}}), \quad (7)$$

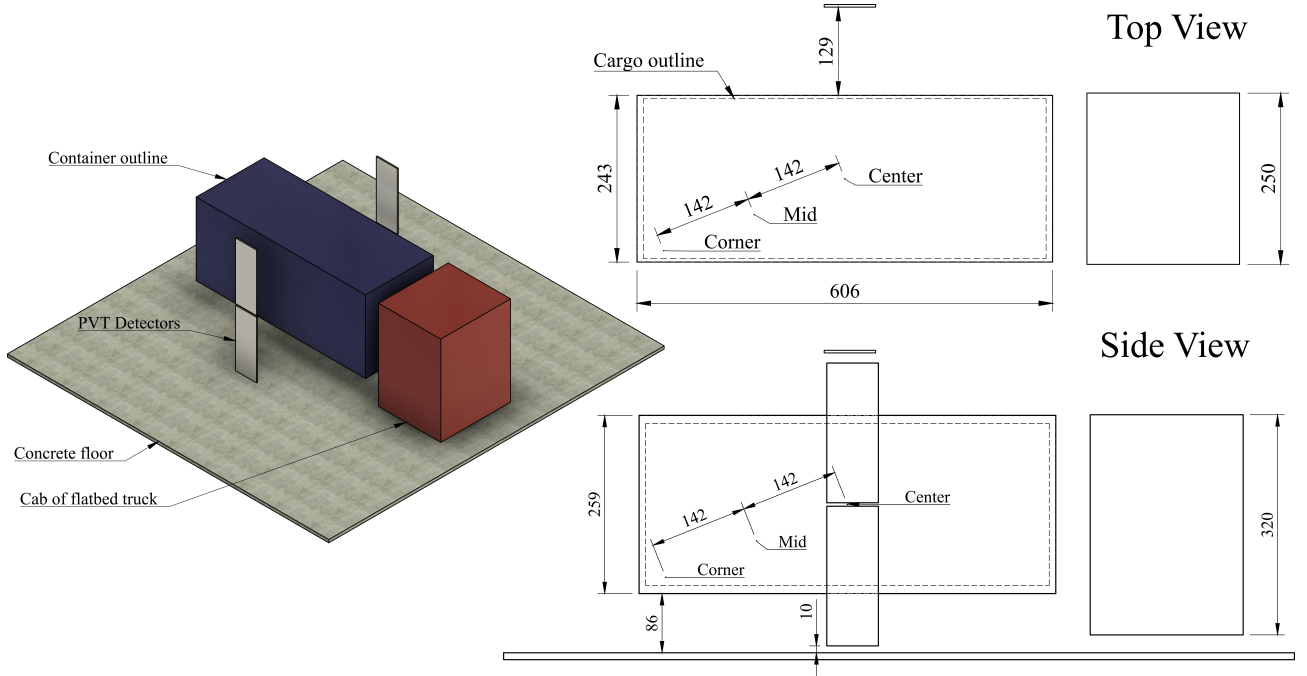


Fig. 1: 3D model of a shipping container (blue cuboid), the cab of a flatbed truck (red), a concrete floor (grey), and four PVT scintillator panels (white). Technical drawings are provided showing the external dimensions of the container, the source positions within the cargo and the cargo outline within the container. All units are in cm.

where ϵ^G is the geometric efficiency, ϵ^I is intrinsic efficiency, \bar{l}^m is the average path length through medium m , ρ^m is the density of medium m and μ^m is the mass attenuation coefficient of medium m at 662 keV. Geometric efficiency describes the solid angle from the source subtended by the detector (divided by 4π) and is calculated stochastically; random γ trajectories are sampled and the fraction that intersect the detector, defined with intersecting planes, is equal to the geometric efficiency. A simple extension of this algorithm allows the path length through the detector volume to be determined for each sampled γ trajectory, which is used to estimate the intrinsic efficiency of the detector for 662 keV radiation. With a method established to determine the average path length through a box by sampling random γ trajectories and seeing where they intersect planes that define the box, it follows that the average path lengths through the container walls and cargo can also be determined.

In approximating the DRF with (7), several factors have been ignored. Firstly, 662 keV γ s scattered to lower energies in the cargo or container walls may deposit energy in the detector. Such ‘buildup’ radiation is not accounted for in (7) and, consequently, the use of (7) results in an underestimate of the number of counts in the detector. Secondly, using an average path length to describe the distance between a voxel center and detector face may be a poor approximation; especially considering the large-area detectors used in this work. Thirdly, the use of $\exp -\bar{l}\rho\mu_g$ as opposed to $\exp -l\rho\mu_g$ is expected to result in an underestimate of the attenuation factor, equivalent to overestimating the attenuation. Clearly, (7) also requires that the cargo material composition, characterised by μ , and distribution are known. This work assumes the cargo fills the internal dimensions of the shipping container and that μ_g^{cargo} is known; improvements to these key assumptions

are explored in Section VI.

C. Algorithm Implementation

All simulations and calculations in this work are performed on a laptop computer with an Intel™ i7 4 core processor and 16 GB of RAM. Generation of RPM measurement data in GEANT4, evaluation of the DRF, and estimation of the average path lengths through the cargo and container walls all require computation time on the order of days. Implementation of the MLEM algorithm variants require only seconds of computation.

To determine the \mathbf{y} values to be used in (5) and (6), the nine measurement datasets (three source positions and three cargo configurations) described in Section III-A are scaled to the desired source activity, 10 MBq, and a constant background count-rate sampled from a Poisson distribution with mean 5000 CPS is added. Each of the MLEM variants is then applied to the datasets to determine $\hat{\mathbf{x}}$ and \hat{b} using the DRF (7) with μ_g^{cargo} equal to the mass attenuation coefficient of iron at 662 keV and ρ^{cargo} equal to the cargo density, which can easily be calculated from the container mass using the cargo distribution assumed in this work.

For all three variants of the MLEM algorithm, the source distribution is initialised as a flat solution with 0.1 MBq in each voxel. In regularised MLEM the effect of the penalty function (3) is to threshold the data, with β roughly defining the threshold position [11]. To determine the optimum β and δ values for use in the regularised algorithm (3) a rough search over the parameters is performed for each source position and cargo combination to determine which values resulted in the highest fraction of the source distribution in the voxels including and adjacent to the voxel containing the true source position. The optimum β values vary from 0.01 to 100, though they are typically larger when the source is localised successfully, whereas δ values are typically 0.001.

Overfitting can be common when using the MLEM algorithm and in this case results in background radiation erroneously being attributed to the source distribution. As a result, indicators of overfitting may be an underestimate of the background count-rate or non-sparse solutions. Defining convergence criteria for MLEM, for example based on the change in likelihood between iterations, is a common method to prevent overfitting. However, in this work a fixed number of iterations, 50, is used for consistency. As is discussed in Section IV there is evidence of overfitting for the unregularised MLEM and regularised MLEM methods, but optimisation of convergence criteria is left for future work.

IV. RESULTS

Firstly, the ability of each variant of the MLEM algorithm to localise the 10 MBq source is considered by calculating the distance between the voxel in the reconstructed solution that contains the maximum activity and the true source position. For regularised and unregularised MLEM with any of the defined cargo, the localisation error when the source is in the centre position is consistently over 1.5 m; one reconstructed solution when the source is in the centre position is shown in Figure 2. Such failure to localise the source is attributed to multiple local minima existing in ℓ due to the symmetry of the problem when the source is in the centre of the cargo. With the source in the corner and mid positions regularised and unregularised MLEM localise the source to between 20 and 80 cm, representing better performance. In comparison, MLEM PS consistently localises the source to within 30 cm at all source positions, except with 0.6 gcm⁻³ cargo and the source in the centre position where the localisation error is 90 cm (shown in Figure 3 (**left**)).

Next, the activity of the reconstructed source distribution is considered. When the source is not ‘accurately’ localised - in the centre position with the regularised and unregularised MLEM methods

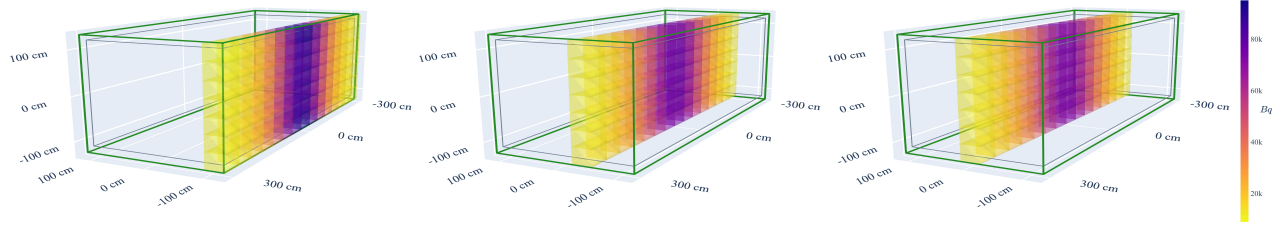


Fig. 2: Three cross-sections of the radioactive source distribution reconstructed using unregularised MLEM with measurements of the 10 MBq source when it is in the centre position with 0.2 gcm^{-3} iron cargo. Localisation error calculated from the voxel with the maximum activity: 1.5 m. Localisation error calculated from the activity weighted voxel position: 0.8 cm.

- the total activity of the reconstructed distribution is still the same order of magnitude as the true point-source. In the corner and mid positions with unregularised and regularised MLEM the sum of the source distribution typically overestimates the total activity of the 10 MBq point-source with ranges of 20-86 MBq and 9-43 MBq, respectively. The fraction of the activity in the most active voxel is higher using regularised MLEM, though is still only 1.5-3.8% and 17.8-27.8% of the total activity for the mid and corner positions, respectively. Along with the visual comparison in Figures 4 and 5, this supports the expectation that the regularised method should result in a sparser, and ultimately more point-source-like solution. Again though, MLEM-PS is more accurate here, with the reconstructed source activity in the point-source solution being between 3.5-56 MBq for all source positions and cargo densities except when the source in the corner position and the cargo density is 0.6 gcm^{-3} , for which the activity is 234 MBq. This last outlier (shown in Figure 3 (right)) grossly overestimates the activity; possible explanations are discussed in Section V.

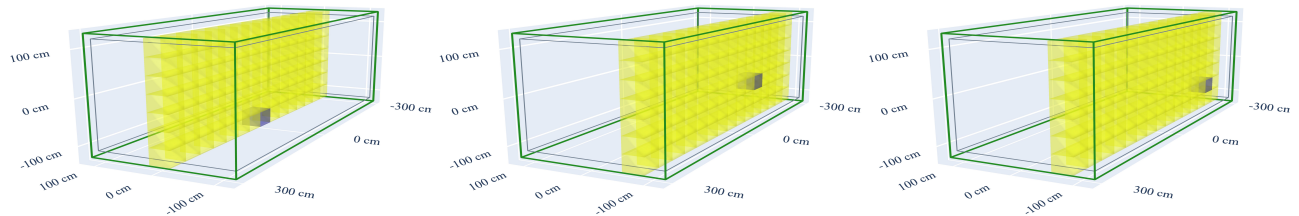


Fig. 3: The point-source solutions reconstructed using MLEM PS when the 10 MBq source is in 0.6 gcm^{-3} iron cargo and the source is: **(left)** in the center position; **(middle)** in the mid position; and **(right)** in the corner position. The associated localisation errors, predicted activities and predicted background CPS are: **(left)** 90 cm, 3.5 MBq, and 5784 CPS; **(middle)** 28 cm, 29.3 MBq, and 5172 CPS; and **(right)** 51 cm, 234 MBq, and 7951 CPS.

Finally, background count-rate estimates are evaluated. Using unregularised MLEM the 5000 CPS count-rate assumed in each detector is typically underestimated by a factor of 10. When considered with the overestimation of the activity, this suggests that the MLEM algorithm may be overfitting the data. Regularised MLEM yields slightly better background estimates and MLEM PS produces the best, with estimates differing from the expected 5000 CPS by factors of 0.03-3.3 and 0.95-5.7 for regularised MLEM and MLEM PS, respectively.

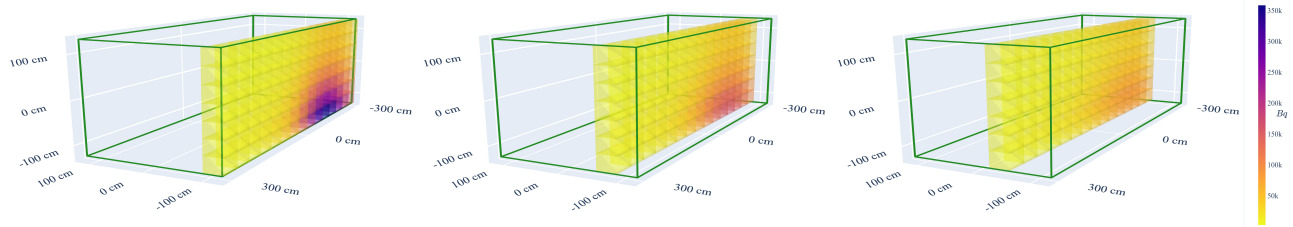


Fig. 4: Three cross-sections of the radioactive source distribution reconstructed using unregularised MLEM when the 10 MBq source is in the mid position and there is no cargo.

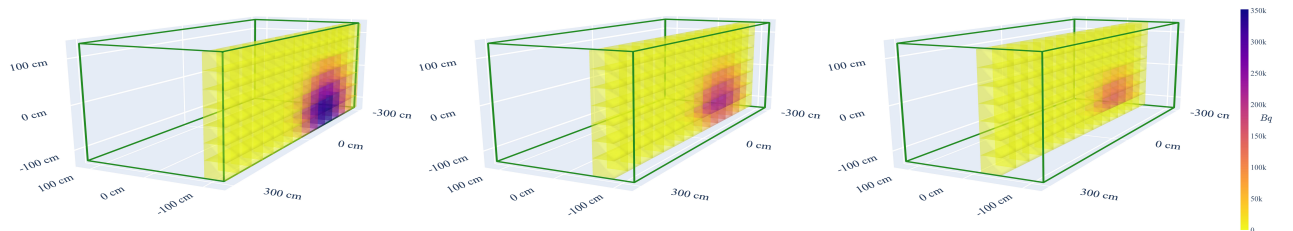


Fig. 5: Three cross-sections of the radioactive source distribution reconstructed using regularised MLEM ($\beta = 100$, $\delta = 0.001$) when the 10 MBq source is in the mid position and there is no cargo.

V. DISCUSSION

This work demonstrates that the MLEM PS method is superior to unregularised MLEM and MLEM regularised with the penalty function (3) for localising a point-source concealed in a shipping container. The MLEM PS method successfully localises the concealed source and predicts the 10 MBq activity and 5000 CPS background count-rate to the correct order of magnitude for containers with no cargo or 0.2 gcm^{-3} iron cargo. However, a concealed source could be disguised in many forms within a container and NORM cargo, such a ceramic materials or cat litter, is more likely to be spread throughout the container [17]. Consequently, it is important to develop the non-point-source variants of MLEM alongside MLEM PS as it is essential to differentiate between these different alarm-inducing sources, and as such algorithm variants that do not constrain the reconstructed distribution are desirable.

It worth noting here that, as the regularised and unregularised MLEM methods result in a solution distributed over multiple voxels, the use of the voxel that contains the maximum activity to calculate the localisation error may belie their performance compared to MLEM PS. If instead the average voxel position weighted by the solution in each voxel is used to calculate the localisation error, a reduction in localisation error is seen across all cargo when the source is in the centre or mid position. While it is promising that the average properties of the solution reflect that of the concealed source, they may not always represent accurate solutions; the use of the average location of the solution suggests the algorithm localises the source well in Figure 2, when clearly the point-source distribution is poorly characterised.

With 0.6 gcm^{-3} iron cargo, which is close to the loading limit of the container, the performance of MLEM PS decreases with large localisation errors and activity estimation errors occurring (see Figure 3). Such a drop in performance at higher cargo densities is expected as the additional attenuation decreases the signal-to-background ratio in the detectors. The drop in performance is compounded by the limitations of the DRF discussed in Section III-B: the omission of buildup

radiation and use of average path-lengths through the cargo are cargo density dependent factors affecting the ability of the algorithm to accurately predict the source activity. Both these factors are expected to overestimate the attenuating effect of the cargo and, therefore, go some way to explaining why all MLEM variants typically result in activity overestimates. Considering the case when the source is in the corner position with 0.6 gcm^{-3} iron cargo, significant activity overestimates of 86, 43, and 234 MBq are produced by unregularised MLEM, regularised MLEM, and MLEM PS, respectively. It is suggested that this is due to the volume of cargo between the source and the two detectors farthest from the source; if a significant fraction of the detected radiation is buildup radiation and the attenuation of the 662 keV source emission is overestimated then, to compensate, the algorithm predicts that the source is a higher activity. Over or under-fitting due to the fixed number of iterations used may also play some role here and the implementation of convergence criteria is a simple extension that will be included in future work.

Fusion of PVT-based RPM measurements with data obtained from spectroscopic detectors, such as NaI(Tl) and LaBr₃(Ce), are likely to form a part of future shipping container screening systems. Such detectors are necessary to identify characteristic emission from any radioactive material within cargo, which is essential to determine at which energies to evaluate the attenuation coefficients used in the DRF (7). By extracting photopeak data from measured high-resolution spectra, the omission of buildup in the DRF is justified for a mono-energetic source, although, coincident events and buildup in the in the presence of a poly-energetic source could inflate the counts in a photopeak. Consequently, spectroscopic detectors can yield further improvements to the MLEM algorithm performance [18], but their associated cost and the limitations on available sizes of means that they are unlikely to replace PVT-based RPMs completely, despite commercial availability.

VI. FUTURE WORK

Whatever detector set-up is implemented, the biggest challenge faced by this method is in characterising the cargo to use in the DRF. So far the simplest possible cargo model is used: homogeneous cargo composed of one material completely filling the container. To extend this method a wider range of cargo distributions and compositions must be considered, that still allows for the average paths lengths through the cargo to be calculated. A cuboidal model of the cargo is proposed with varying height cargo. Assuming the container is filled from the base, the cargo fills the entire floor space of the cargo, and the centre of mass (CoM) of the container can be obtained, the height of the cargo can be determined. Such a method requires the CoM of the container (in 3D) to be calculated, which poses a further challenge, but is conceivable given the lifting processes involved in transporting shipping containers.

Determining the composition of the cargo, which must be known to select the attenuation coefficient used in the DRF, poses another considerable challenge. Relying on cargo manifest information assumes the trust and competence of the person(s) loading the container and filling in the manifest information. To overcome this problem, a confidence interval around the algorithm outputs could be constructed based on the ‘expected’ contents of the container, whether that be estimated from cargo manifest information or from a container’s typical contents [14]. Such an approach may result in more false-positive alarms due to the sensitivity (exponential dependence) of the algorithm to the μ_g^{cargo} used; overestimating μ_g may result in significant activity overestimates.

Beyond improving the cargo and DRF model, future work will consider a wider variety of sources. A key performance metric of shipping container screening systems is their ability to differentiate between nuisance and legitimate threat sources, therefore, the ability of the algorithm to characterise nuisance cargo must be evaluated.

VII. CONCLUSIONS

The abilities of three MLEM algorithms to accurately localise and predict the activity of a 10 MBq 662 keV point-source concealed in a shipping container filled with iron cargo and passing through a PVT-based RPM are compared. Using simple assumptions of the cargo distribution and composition reasonable localisation performance is achieved, with the best results occurring when knowledge that the source distribution is a point-source is provided. PVT-based RPMs favoured for their low cost and large available sizes are likely to form a crucial part of future shipping container screening systems. Resultantly, demonstrating that accurate source location, source activity, and background count-rate estimation is achievable with existing plastic scintillator-based RPMs indicates how primary phase screening of shipping containers can be further optimised to reduce the occurrence of false-positive or false-negative alarms in the future.

REFERENCES

- [1] OECD, <https://www.oecd.org/ocean/topics/ocean-shipping>, Accessed: 2023-03-21.
- [2] American Nuclear Society, <https://www.ans.org/news/article-4703/cs137-sealed-source-lost-in-western-australia/>, Accessed: 2023-03-21.
- [3] British Broadcasting Corporation (BBC), <https://www.bbc.co.uk/news/world-africa-64972945>, Accessed: 2023-03-21.
- [4] E. L. Connolly *et al.*, *Journal of Nuclear Engineering 2021*, Vol. 2, Pages 246-280, vol. 2, no. 3, pp. 246–280, Aug. 2021. DOI: 10.3390/JNE2030023.
- [5] L. Marques *et al.*, *Sensors*, vol. 23, no. 1, 2023. DOI: 10.3390/s23010329.
- [6] C. Thomay *et al.*, *IEEE Transactions on Nuclear Science*, vol. 62, no. 4, pp. 1837–1848, 2015. DOI: 10.1109/TNS.2015.2441776.
- [7] B. D. Geelhood *et al.*, in *2003 IEEE Nuclear Science Symposium. Conference Record*, IEEE, 2008, pp. 513–517. DOI: 10.1109/nssmic.2003.1352095.
- [8] D. Hellfeld *et al.*, *IEEE Transactions on Nuclear Science*, vol. 66, no. 9, pp. 2088–2099, 2019. DOI: 10.1109/TNS.2019.2930294.
- [9] M. S. Bandstra *et al.*, *IEEE Transactions on Nuclear Science*, vol. 68, no. 11, pp. 2637–2646, 2021. DOI: 10.1109/TNS.2021.3113588.
- [10] E. A. Miller *et al.*, *IEEE Transactions on Nuclear Science*, vol. 62, no. 5, pp. 2234–2244, 2015. DOI: 10.1109/TNS.2015.2474146.
- [11] D. J. Lingenfelter *et al.*, *Computational Imaging VII*, vol. 7246, 72460F, 2009. DOI: 10.1117/12.816961.
- [12] A. Krol *et al.*, *IEEE Transactions on Medical Imaging*, vol. 20, no. 3, pp. 218–232, 2001. DOI: 10.1109/42.918472.
- [13] International Organization for Standardization (ISO), ISO 668:2020, 2020.
- [14] M.-A. Descalle *et al.*, in *2006 IEEE Nuclear Science Symposium Conference Record*, vol. 1, IEEE, 2006, pp. 275–280. DOI: 10.1109/NSSMIC.2006.356155.
- [15] International Atomic Energy Agency, *IAEA safety standards series*, vol. No. RS-G-1, no. July, p. 70, 2005.
- [16] S. Agostinelli *et al.*, *Nuclear Instruments and Methods in Physics Research Section A: Accelerators, Spectrometers, Detectors and Associated Equipment*, vol. 506, no. 3, pp. 250–303, Jul. 2003. DOI: 10.1016/S0168-9002(03)01368-8.
- [17] J. Baciak *et al.*, Jan. 2011. DOI: 10.2172/1036932.
- [18] E. L. Connolly *et al.*, *Nuclear Technology*, 2023, (in press). DOI: 10.1080/00295450.2023.2198473.